MECHANIKA TEORETYCZNA
I STOSOWANA
Journal of Theoretical
and Applied Mechanics
2, 34, 1996

NEW APPLICATIONS OF THE HOPKINSON PRESSURE BAR TECHNIQUE TO DETERMINING DYNAMIC BEHAVIOUR OF MATERIALS

LEOPOLD KRUSZKA

Military University of Technology, Warsaw

WOJCIECH K. NOWACKI

Institute of Fundamental Technological Research, Warsaw

e-mail: wnowacki@ippt.gov.pl

Experimental results of dynamic uniaxial compression, tension and shearing tests on brittle and metals at high strain rates are presented. In these dynamic investigations a standard Hopkinson bar device with a pneumatic launcher was used. Various testing configurations and accessories of the set-up are shown here. It makes possible to determine dynamic behaviour of materials in different modes of an examination having the above test stand only.

1. Introduction

The main aim of this paper is to present some new research possibilities of Hopkinson pressure technique for determining dynamic behaviour of various materials. The purpose is not only to show the dynamical properties of investigated materials, but also to give information useful for completing various test configurations using a standard modified Hopkinson bar apparatus in order to enable investigations in different modes of testing at high strain rates; i.e., in compression, tension, or shearing.

First, test results together with fracture mechanisms obtained from the dynamic compression (high strain rates of the order of $10^3\,s^{-1}$) of brittle photoelastic material are compared with those from the static compression. Four

slenderness ratios of uniaxial short cylindrical specimens were dynamically tested in the standard Split Hopkinson Pressure Bar (SHPB), (cf Kruszka et al. (1992b)).

Next, the deformation and the surface temperature fields in long cylindrical specimens (e.g., aluminium alloys) of different lengths are experimentally determined in the Taylor impact tests, using the configuration of SHPB for those tests and a thermovision set (cf Kruszka and Nowacki (1995)). The specimen strikes normally an obstacle with the initial velocity v_0 undergoing considerable dynamical deformation. The strain rates were of the order of $10^2 \div 10^3 s^{-1}$. It was fount out that most suitable measuring technique (of temperature distribution in dynamically deformed specimens) was a non-contact measurement based on the Infrared Radiation (IR) detection (cf Klepaczko and Kruszka (1994)).

Then, further modification of the SHPB system is presented, which permits testing of a long cylindrical specimen made of an elastin-brittle materials under pure dynamic tension. It is a new type of test in which the specimen is subjected to a controlled axial impact. The tests performed on a microconcrete provided a unique measure of the uniaxial strength. During experiments, the phenomenon of multiple spalling are registered using above mentioned thermovision set.

Finally, a new dynamic plane shear test is discussed. It uses a new shear device, loading and displacements of which are controlled by the SHPB used in the compression configuration. This device allows the performance of tests under plane shear state for a specimen having the form of slab, as metal sheets for instance. Furthermore, large deformation can be reached without any localisation of the strain, in contrast with the torsion test made on a thin tube specimen.

2. Dynamic compression

The SHPB (cf e.g. Klepaczko (1971)) was first designal to study plastic properties of metallic disc specimens under compression at high strain rates. It has wide-spread application also to the studies of dynamic behaviour of other materials such as plastics and brittle materials; in particular, rocks and concrete (cf Bhargava and Rehnstrom (1977); Buchar and Dusek (1975); Chou et al. (1973); Christensen et al. (1972); Klepaczko (1971) and (1983); Krzyszton et al. (1986); Lindholm et al. (1974); Lundberg (1976); Maiden and Green (1966); Malvern et al. (1986)). This procedure makes it possible to observe

the whole process of dynamic loading of a cylindrical specimen including an instant of fracture and subsequent fragmentation leading to final destruction of the specimen.

Locally available materials were used to make the photoelastic brittle material: epoxy resin Epidian 2 and distilled rosin. The method of preparation was described by Wolna and Kruszka (1991). A series of cylindrical specimens were made, of the diameter $d_0 \approx 17\,\text{mm}$ and the heights $h_0 = 0.5d_0$; d_0; $1.5d_0$; $2d_0$, respectively. The average specific weight of the material was $\gamma = 11.2\,\text{kN/m}^3$, the average Brinell hardness amounted to $H_B = 23.2$. The method of ultrasonic elastometry made it possible to determine the following average values of material constants:

- Propagation velocities of elastic waves; for longitudinal waves $c_L = 2480\,\text{m/s}$, for transverse waves $c_T = 1096\,\text{m/s}$
- Lame constants: $\lambda = 4410\,\text{MPa}$, $\mu = 1410\,\text{MPa}$
- Young modulus $E_0 = 3770\,\text{MPa}$, bulk modulus $K = 5240\,\text{MPa}$
- Poisson ratio $\nu = 0.38$.

The following notation of specimens was adopted:

- Slenderness $s = 0.5$; 1.0; 1.5; 2.0 by means of letters A, B, C, D
- Consecutive casts: I $\div$ V
- Consecutive numbers of specimens of the same slenderness $1 \div 8$.

Static compression was realised in a mechanical testing machine with the constant velocity of its traverse $v_t = 0.07\,\text{mm/min}$. Global strain rate in the deformation process was $\dot{\varepsilon} = vt/h$. Diagrams of the compressive force F versus displacement $\Delta h = h_0 - h$ (change in the distance between platens) were produced. Next, the average nominal stresses $\sigma = F/A_0$ (A_0 – initial cross-section of a cylinder) as functions of global strain $\varepsilon = \Delta h/h_0$ were obtained.

In dynamic investigations short cylindrical specimens of various height-to-diameter ratios were subjected to compressive action of above $20\,\mu\text{s}$ duration. A schematic diagram of the dynamic test stand is shown in Fig.1. This set-up consists of the following elements: a pneumatic launcher W of bar projectiles 1, an incident bar 2 in which longitudinal elastic compression wave of a strain in time $\varepsilon_I(t)$ is generated, a first part of it is reflected as a tension wave $\varepsilon_R(t)$, a transmitting bar 3 in which the second part of input wave

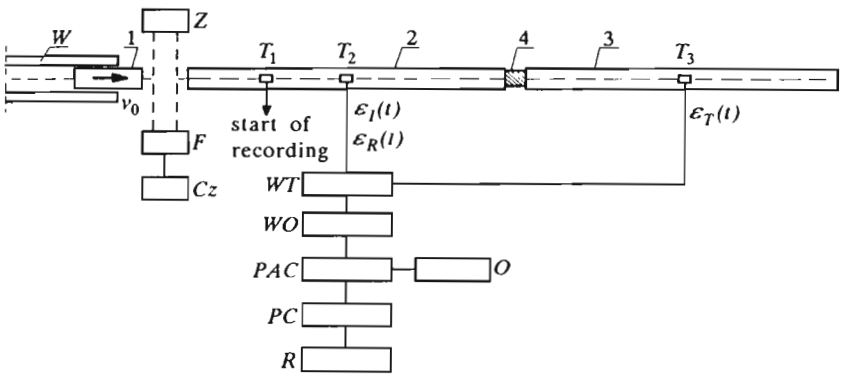

Fig. 1. Standard SHPB apparatus

$\varepsilon_I(t)$ propagates as a compression wave $\varepsilon_T(t)$ after a transition across a specimen 4. Between the measuring bars 2 and 3 there is the test specimen 4 which undergoes deformation, damage and fracture.

The following letter symbols signify accessories of the test stand: Z – source of light, F – photodiodes, Cz – timer to measure transit time of the projectile between measurement points of the impact velocity v_0, T_1, T_2, T_3 – strain resistance gauges, WT – strain gauge amplifier, WO – operational amplifier, PAC – analogue-digital storage register, O – oscilloscope, PC – microcomputer, R – XY recorder or graphic printer.

Detailed description of static and dynamic tests carried out is given by Kruszka et al. (1992a,b). Relevant results of dynamic experiments are shown for four selected specimens: CIII/1, CIII/3, DIV/2 and DVI/7 in Fig.2a ÷ Fig.2d, respectively. The given curves comprise: stress-strain $\bar{\sigma} - \bar{\varepsilon}$ diagrams, stress $\bar{\sigma}$ and strain rate $\dot{\bar{\varepsilon}}$ diagrams as functions of time t and strain rate-strain $\dot{\bar{\varepsilon}} - \bar{\varepsilon}$ relationships in terms of averaged values (dashes over symbols). Dynamic stress-strain curves are presented in Fig.3 for seven specimens with various slenderness and subjected to various strain rates. Static curve for $s = 0.5$ is also shown. Considerable increase in dynamic Young modulus can be observed. Dynamic unloading can be clearly seen in specimens of lower slenderness ($s = 0.5$ and $s = 1.0$). The tested material is found to be strain-rate sensitive (compare for $s = 0.5$: $= 1.4 \cdot 10^{-6}\,\mathrm{s}^{-1}, 390\,\mathrm{s}^{-1}, 680\,\mathrm{s}^{-1}$). However, the largest stresses were those reached under static loading.

The described experiments have enabled the brittle photoelastic material subject to compression to be studied within two ranges of the strain rate: low (static tests) and high (dynamic tests). The material is found to be strain

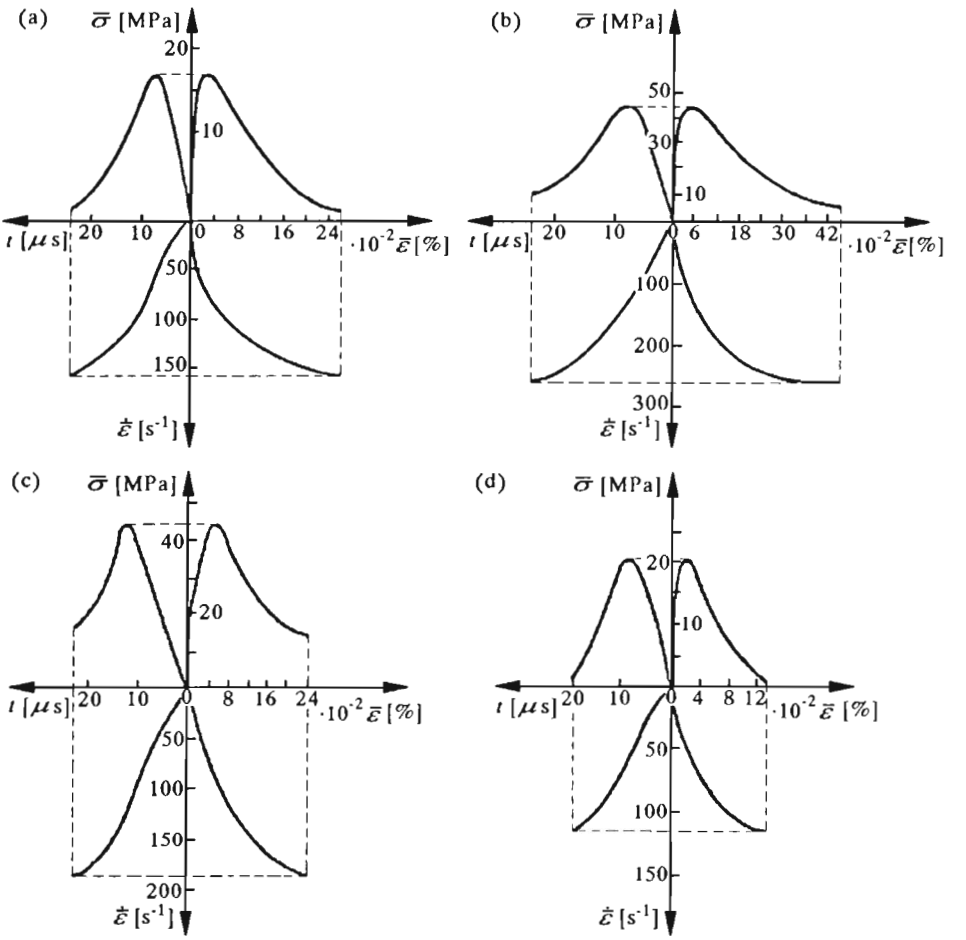

Fig. 2. Diagrams of stress-strain, stress-time, strain rate-time and strain rate-strain for specimens: (a) CIII/1 ($s = 1.5$); (b) CIII/3 ($s = 1.5$); (c) DIV/2 ($s = 2$); (d) DIV/7 ($s = 2$) under dynamic load

rate sensitive both in the elastic range (considerable increase in the Young modulus) and in the plastic range (different dynamic characteristics). Larger elastic deformations are noticed under static than under dynamic loading. This can be explained by the fact that at low strain rates not only purely elastic but also viscoelastic strains have enough time to develop. For high strain rates the elastic strains are of almost completely instantaneous nature. The increase in strain rate being observed affects the increase of material elasticity accompanied by its short-term strength decrease. The latter fact is explained

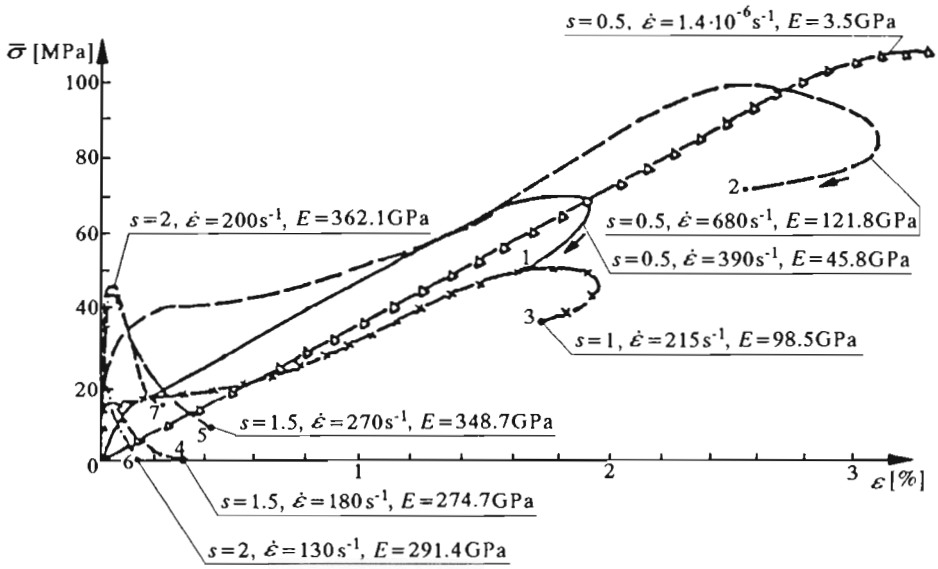

Fig. 3. Dynamic stress-strain $\sigma - \varepsilon$ curves for specimens of various slenderness s and subjected to various strain rates $\dot{\varepsilon}E_0$; E – static and dynamic Young moduli. Notation of specimens: 1 – AII/2; 2 – AV/6; 3 – BII/2; 4 – CIII/1; 5 – CIII/3; 6 – DIV/7; 7 – DIV/2

by a ductile-brittle character of the failure under static load and a brittle one observed under dynamic load.

The geometry of specimens has also been found to have considerable effect on the stress-strain relationships and the fracture mechanisms. In dynamic tests the $\sigma - \varepsilon$ curves turned out to be different for slender specimens ($s > 1$) from those obtained for short specimens ($s \leq 1$). The effects of slenderness in static tests were observed not earlier than on the post-critical branch of $\sigma - \varepsilon$ curve (after the short-term strength has been reached); the shape of this branch strongly depended on the failure mechanism of the specimen. In the dynamic tests defects and fracture are accompanied by longitudinal and transversal cracks, the latter being present only in the specimens of the slenderness $s > 1$. Regions of defects and failure originate from the loaded end of specimen and, as well as, the intensity of defects, depend on the loading rate. For specimens with $s = 0.5$ failure occurs along the whole height. In the static tests, compression failure prevails for $s > 1$, skew shears and longitudinal splitting are present for $s = 1$, cracks are accompanied by the surface spalling for $s = 0.5$. Each of the above mechanisms is characterised by a different post-critical $\sigma - \varepsilon$ branch. Fragmentation in the case of static load

is finer than in the dynamic case. A detailed description of degradation of the investigated material at various strain rates is given by Kruszka et al. (1988).

Brittle materials are characterised by initiation of microcracks upon loading followed by the desintegration of a testpiece. That is why a rigidity of a mechanical loading system plays an important role in the tests (cf Bauer (1982)). If the post-failure characteristic of a brittle material has larger slope than that of the loading system, a sudden desintegration of the material will occur. Thus considerable rigidity of the testing machine is advisable to enable accurate measurements of the material properties during the falling branch of the load-displacement curve and to obtain information on both ascending and descending branches of the process. The SHPB as the testing machine used in this type of experiments is found to be rigid enough.

3. Thermomechanical Taylor impact test

The testing stand was based on the SPHB system and the AGA 680 thermovision set (TS). Taylor impact tests were performed using right cylindrical specimens as projectiles with the Hopkinson measuring bar as the target so that load/time data were recorded during the tests. A schematic diagram of the dynamic test stand is shown in Fig.4. This set-up consists of the same elements that shown in Fig.1, but without the transmitting bar 3. This experimental arrangement is completed by a thermovision camera KT.

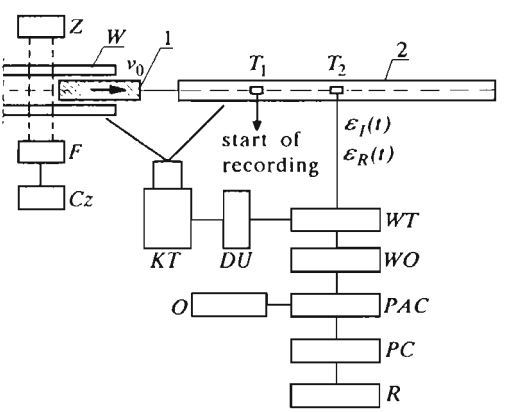

Fig. 4. Schematic diagram of the Taylor impact test

Selected elements of this stand are shown in Figure 5. The aluminium

specimen 1 moved inside a barrel of the pneumatic launcher W towards the obstacle 2 that was the incident bar of SHPB. The impact velocity v_0 was determined measuring the time between crossings of two parallel light beams by the impinging specimen. These velocities were about $75 \div 150\,\mathrm{ms}-1$.

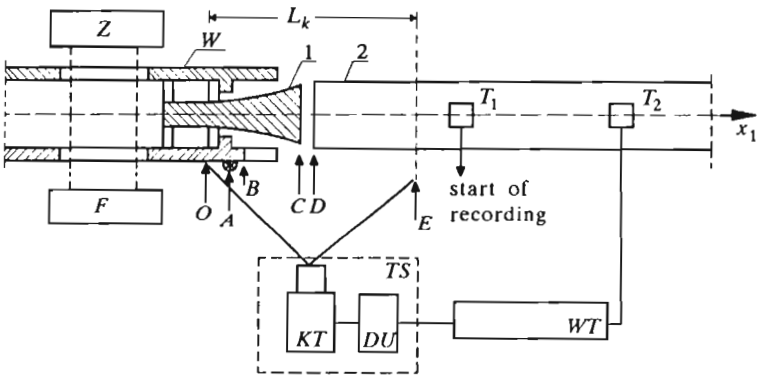

Fig. 5. Selected elements of the testing stand

The specimens were made of a soft aluminium alloy (95.5% of pure aluminium). The cylindrical specimens were $d_0 = 11$ mm in diameter and $l_0 = 80$, 95, 115 mm in length. Two teflon rings were intended to ensure the coaxial motion of the specimen inside the gun tube (Fig.6). The specimen had no side contact during its motion. It was then possible to avoid any friction effect and related heating, thus there was no misinterpretation of the measurement results. Circumferential lines parallel to the specimen face were marked every 5 mm on the lateral surface of cylinder in order to measure the permanent longitudinal deformations. The lateral surface of cylinder of the specimens were coated with soot to improve the emission of heat, and thus to obtain more intense signals which were displayed as thermovision images on the monitor screen.

Figure 7 illustrates the wave propagation in the specimen and in the incident bar of SHPB on the phase plane (X_1, t). The lines on the specimen correspond to the cycles during in which the strong discontinuity wave propagates through the specimen. On the other hand, in the incident bar the compressive elastic wave is affected by the impact of this specimen. This wave arrives at the other end and goes back within this bar as a tensile elastic wave. The potentiometric strain gauge system T_2 is mounted at the mid-length of the incident bar. Its signal is produced in the amplifier WT and recorded in one of the channels of the analogue-digital storage register PAC (see Fig.5).

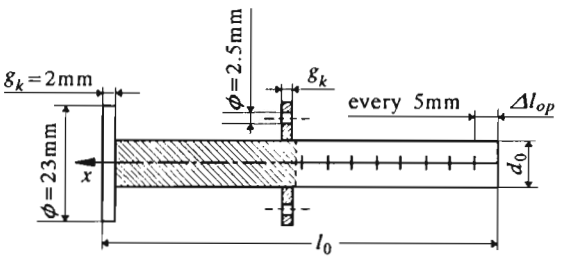

Fig. 6. Long cylindrical specimen with two teflon rings

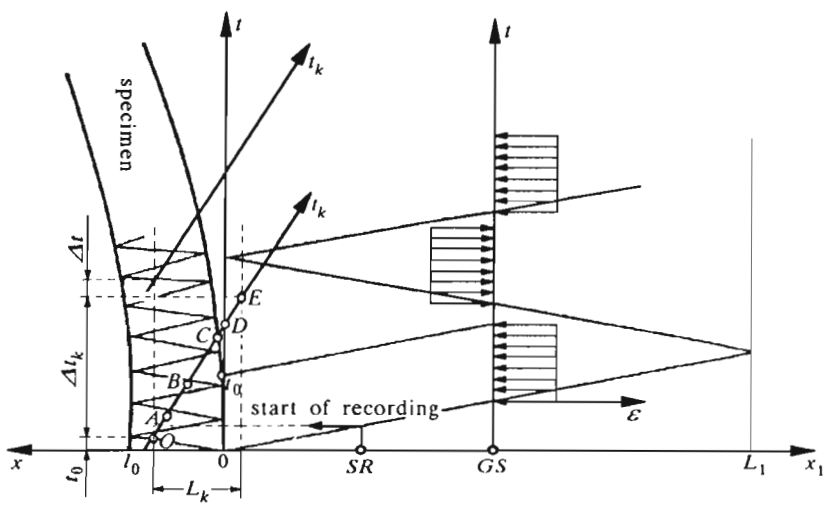

Fig. 7. Images of wave propagation in specimen and incident bar. Infrared radiation power was recorded on the line *O-E*

In order to determine the temperature distribution in the most deformed part *B-C* of the specimen, the impact space was observed by the thermovision camera *KT*. The thermovision image is a scanning result of an observed surface by two prisms rotating vertically and horizontally. This image on a screen of the display unit *DU* corresponds to the *IR* power surface distribution. Duration of the deformation process was too short (about 0.2 ms) to observe the accompanying increase of temperature on the whole image (60 ms). Hence, in our experiment the horizontal prism was stopped. It was then possible to obtain the frequency of image line equal to 1.6 kHz. The registering time of this line on the screen was 625 μs. This line corresponds to the generating line of the cylindrical specimen. The investigated thermomechanical process

was axially symmetric. Such an approach was sufficient to properly describe the above impact process.

An indicator of constant temperature A was placed in the observation space of the camera. The temperature of this indicator need not to be known. This temperature played a role of constant reference level.

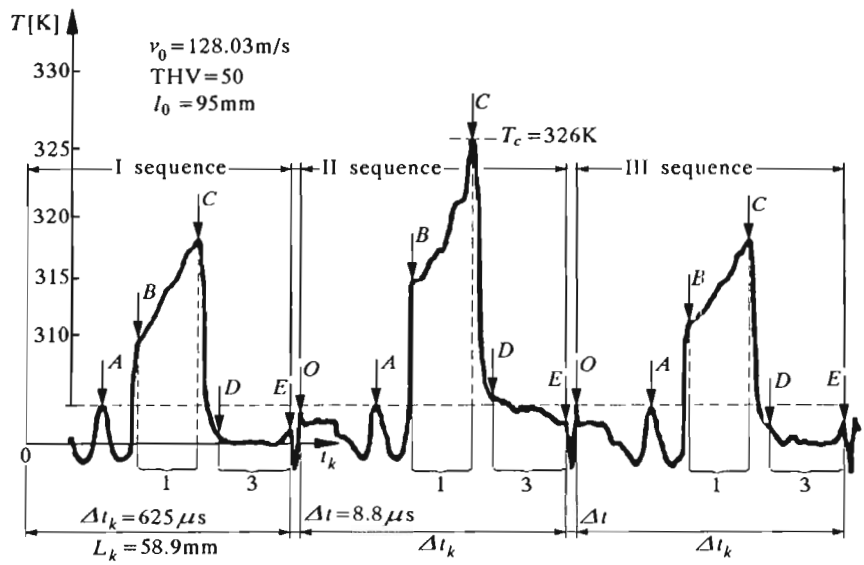

Fig. 8. Temperature distribution along the observed segments

Using the calibration of temperature measuring set it was possible to assign the absolute temperature values to the recorded IR power distribution emitted by the points of the specimen meridian. Fig.8 illustrates the registration of temperature distribution along the observed segment of the length $L_k = 58.9$ mm. By changing the frequency of oscilloscope time base, it was possible to record the sequential time intervals of $\Delta t_k = 625$ μs in duration. The maximum heating of the specimen surface occurred in the second observing sequence, which proved the thermal inertia of the specimen. In this figure Δt denotes the time interval of jump of the thermovision camera prism to the next observation sequence. This experiment allowed determination of the maximum temperature values T_c in function of the impact velocities v_0 in the considered dynamic deformation process. The non-dimensional increments of temperature $\Delta\bar{T}_c = [(T_c - T_0)/T_0] \cdot 100\%$ at the specimen's end are shown in Fig.9 vs. the impact velocity v_0 for different slenderness ratios. T_0 is the room temperature.

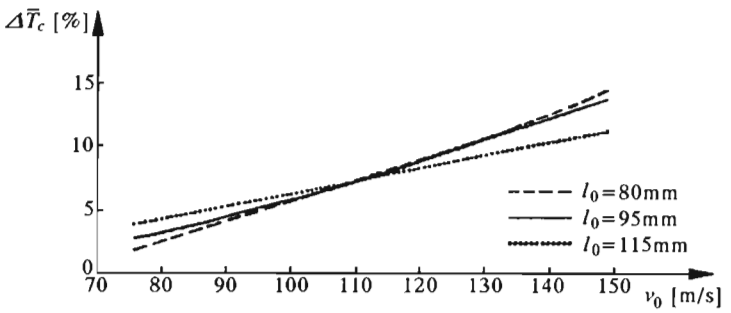

Fig. 9. Increments of the temperature in the end of the specimen vs. impact velocity

Using this testing configuration it was possible to determine the time t_c of contact of the specimen with the obstacle, from the process of deformation registration in the receiving bar of the SHPB system. Fig.10 shows the variation of the contact time with v_0. This time increases quasi-linearly with the increase of v_0.

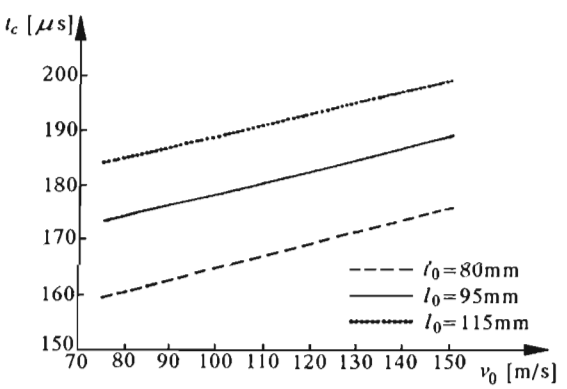

Fig. 10. Times of contact of the specimen with the receiving bar vs. the impact velocity

On the basis of the microscopic measurements, the permanent deformations are determined in the Almansi-Hamel measure ε^A. In Fig.11 the increase in the permanent longitudinal and transversal deformations of the specimen ($l_0 = 95$ mm) in the function of non-dimensional length $\bar{X} = X/l_0$ for six different values of the impact velocity v_0 are shown. Fig.12 shows the influence of recrystallisation upon the distribution of the permanent longitudinal and transversal deformations for specimens of the length $l_0 = 95$ mm striking with similar velocities. In the case of non-annealed aluminium it can be observed

the largest deformations in the front part of the specimen and considerably smaller ones in the remaining part of the specimen, for $\bar{X} > 0.2$.

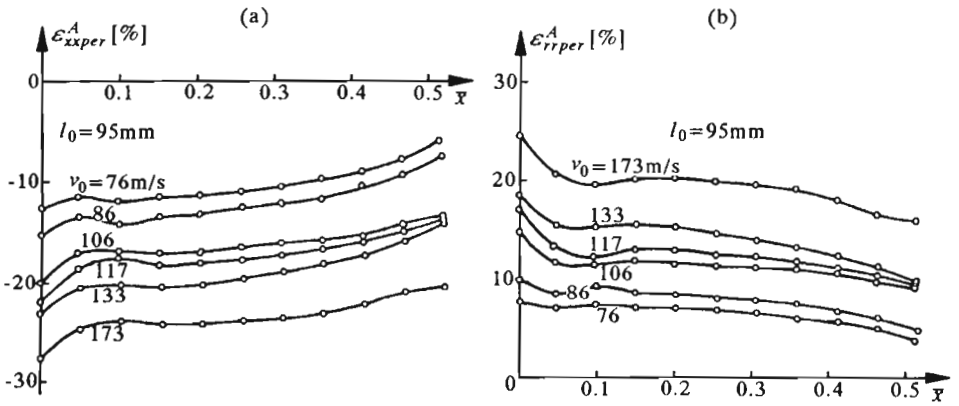

Fig. 11. Permanent longitudinal (a) and radial (b) deformations versus $\bar{X} = X/l_0$

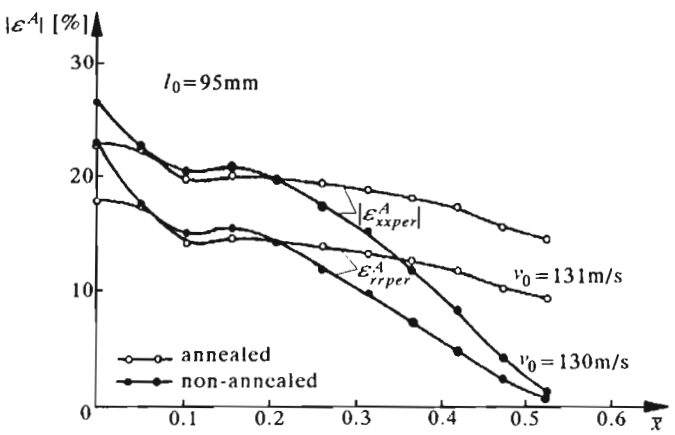

Fig. 12. Permanent deformations for non-annealed and annealed aluminium specimens, respectively

From the experimental results it can be also noticed that the initial length of the specimen (impact at the same velocity) exerts no appreciable influence on the permanent deformation. The initial length of the specimen does not affect visibly the reduction l/l_0 of the specimen, and the permanent deformations of the specimen in the function of impact velocity v_0, (cf Kruszka and Nowacki (1995)). The strain and temperature field determined experimentally

is useful to verify the theoretical model of the cylindrical specimen impinging the obstacle.

4. Spalling test

Brittle materials fail under dynamic loading mainly in the spalling mode. Various versions of the SHPB apparatus developed for direct tensile tests (cf Klepaczko and Kruszka (1994)) are equally non-suitable for tensile experiments of those materials due to complicated shapes of specimen grips which cause additional scatter and high costs. The set-up combines the SHPB principles of pulse initiation and its measurement with the tensile dynamic loading arising in result of the reflection of the compressive stress wave from the specimen free end, typical for spalling experiments. The slenderness ratio of about 20 (cf Najar (1994)) and a carefully selected pulse profile result in the spall developing sufficiently far away from the reflection point to ensure the uniaxial stress. The compressive pulse transmitted into the specimen propagates here without causing material damage. Upon its arrival at the free end it gets reflected as a tensile pulse and superposed upon the still arriving tail. The resulting stress distribution leads to tensile stresses increase with the distance from the free end and fast growing in time. Wherever the peak value of resulting stress distribution reaches the level of tensile strength of the material, spalling occurs. The part of the pulse and the momentum trapped in the fragment causes in most cases secondary in-flight fractures based on the same mechanism, provided sufficient pulse amplitude. The knowledge of the site of the primary spall, allows determination of its spall strength.

The configuration of performed physical experiment on dynamic tension of long cylindrical specimens is shown in Fig.13a. The projectile 1 strikes the long measuring bar 2 affecting the longitudinal wave propagation.

Its amplitude and the pulse duration are registered by a strain gauge as the $\varepsilon_I(t)$ pulse. This wave, loading the specimen 4, is partially transmitted along the specimen as the $\varepsilon_T(t)$ pulse, and is partially reflected from the specimen face as the $\varepsilon_R(t)$ pulse. It is the result of different cross-sections and material properties of the specimen and the measuring bar. It is possible here that the specimen is glued to the bar or it is only in contact with this bar. At the contact between the measuring bar 2 and the specimen 4 the following condition should be satisfied

$$A_0\sigma_T\Big|_{x=0} = A_H(\sigma_I + \sigma_R)\Big|_{x=0} \tag{4.1}$$

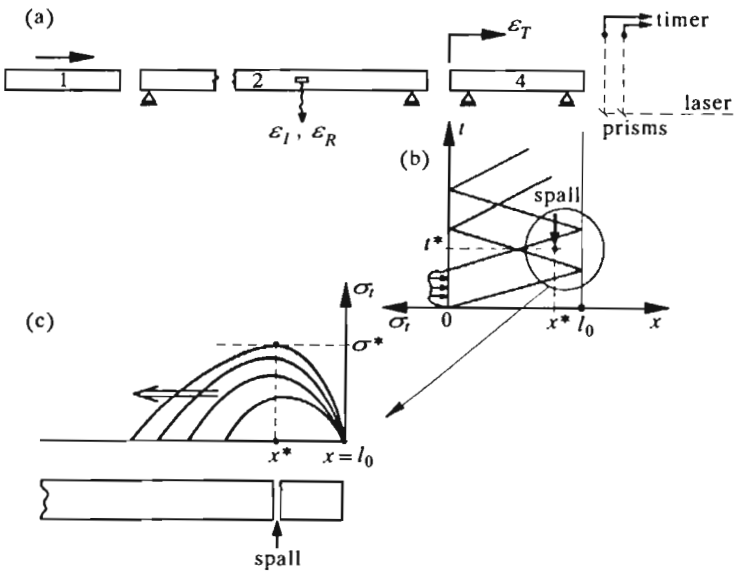

Fig. 13. Scheme of the performed experiment; (a) – configuration of the Hopkinson bars and specimen, (b) – image of elastic wave propagation in specimen, (c) – reflection of waves from free end of specimen

where $\sigma_T = E\varepsilon_T$, $\sigma_I = E_H\varepsilon_I$, $\sigma_R = E_H\varepsilon_R$; A_0, A_H and E, E_H are the cross-sections and the Young moduli of the specimen and the measuring bar, respectively.

In order to generate very short-term loading pulse $\varepsilon_I(t)$ without any peaks, one used short projectiles 1. Their length L_p was most often equal to 20 mm or 25 mm and their diameter $D_p = 20$ mm and 22.8 mm – see Fig.16. At half length of the Hopkinson measuring bar 2 ($L_H = 1000$ mm, $D_H = 20$ mm) there are the pair of strain gauges T_1 and T_2 – see Fig.14, in order to register oscillations of the loading pulse $\varepsilon_I(t)$ and the reflected pulse $\varepsilon_R(t)$. The spall fragments formed due to loading pulse were get together into the container designed for this purpose, lined with a soft material. It protected these fragments against their further damage. The compressing pulse $\sigma_t(t)$ in the specimen – Fig.13b, which comes to the free end of the specimen ($x = l_0$), undergoes a reflection and reverses progressively its sign as the stretching one. Reflected waves have their pulse amplitude higher and higher – Fig.13c. It can occur, that at a certain cross-section it was exceeded the tensile strength. At the moment, when the stress reaches the maximum critical value σ^* (the spall stress), the brittle fragment of length $l_s = l_0 - x^*$ suddenly breaks away from the remainder of specimen material and displaces in the x direction.

At some changes in $\sigma_t(t)$ stresses, it can form more than one spalling – see Bierwirth and Najar (1992).

The set-up (Fig.14), used in this experiment, consists of the same elements which are shown in Fig.1, but without the transmitting bar 3. The long cylindrical specimen 4 is placed at the free end of measuring bar 2 lined along the axis of the set-up. The final sector of the specimen was observed by the thermovision camera KT. The principle of its working is the same as during the Taylor impact test, i.e., it works as the linear camera. Its task is to record an infrared radiation power along the generating line of the heated specimen. It causes that the specimen surface gives very distinct signal in comparison with the background. In case of spalling occurrence, a material failure of the specimen is sharply outlined. From the registered observing sequences of infrared radiation power versus time one can easy estimate the spall location and spall speeds of the fragments.

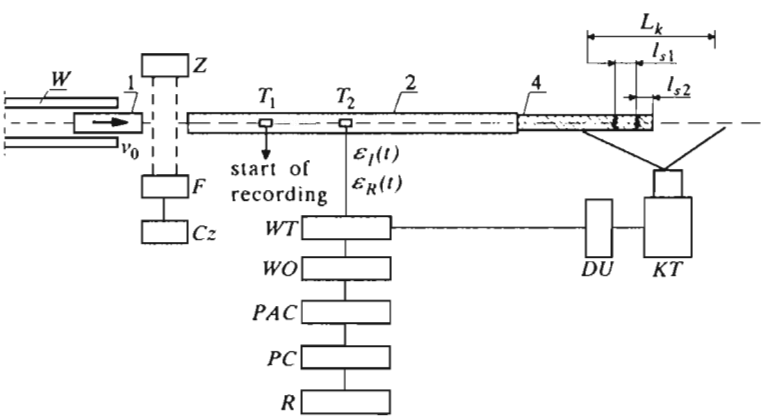

Fig. 14. Experimental arrangement

The compressive pulse $\varepsilon_I(t)$ induced in the measuring Hopkinson bar 2 by projectile 1 impact as it travels along gets registered at the gauge stations T_1, T_2 and stored. The same happens to the reflected pulse $\varepsilon_R(t)$ resulting from the difference of the effective impedance between the measuring bar and the specimen.

Rods of the microconcrete of 16.5 mm and 18.4 mm in diameter wfere used in these impact tests. The lengths of specimens were 270 mm, 292 mm and 298 mm, respectively. The example of the observation about the spalling strength test with the projectile of the length $L_p = 25$ mm and the diameter $D_p = 22.8$ mm at the impact velocity $v_0 = 25.8$ m/s, is presented here. One

can easy calculate the tensile strength σ^* of the investigated material using the following formula

$$\sigma^* = -\frac{A_H E_H(\varepsilon_I - \varepsilon_R)}{A} \tag{4.2}$$

where A_H, E_H are the cross sectional area and the Young modulus of the measuring bar and A is the specimen cross sectional area. Its value is equal to -86.5 MPa. Fig.15 illustrates the registration of the infrared radiation power distribution along the observed segment of the length $L_k = 195$ mm. In this figure are also shown the evaluated spall lengths l_{s1}, l_{s2} of successive occurring spall fragments and the initial spall speed of the first one v_s, which averages 9.4 m/s. According to the well-known relationship one can also estimate the tensile strength σ^* as follows

$$\sigma^* = -\rho_0 c_L v_s = -85.3 \text{ MPa} \tag{4.3}$$

where

ρ_0 – mass density

c_L – wave speed in the material of specimen.

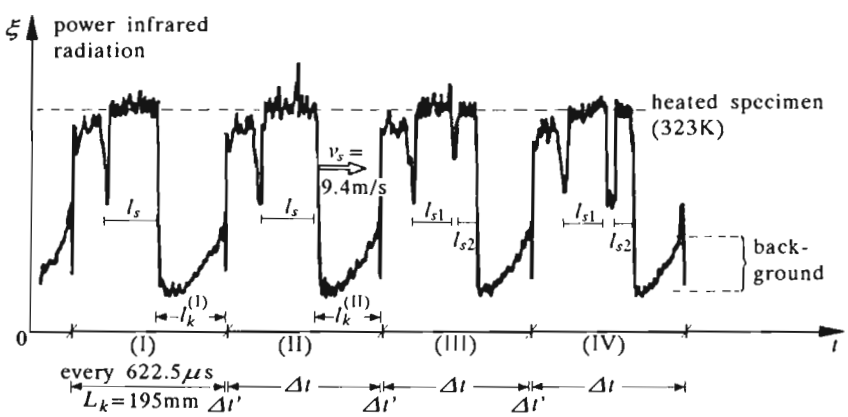

Fig. 15. Distribution of infrared radiation power along selected horizontal line of the observed segment in four time cycles

Within the framework of the treatment of the uniaxial waves in long rods, on the assumption of linear elastic-brittle response of the tested materials one can deduce two ways, taking advantage of the experimental data of the stress pulse transmitted into the specimen, the location of the spalling plane and the initial spall speed, the level of stress developed at spalling. Collective representation of experimental results of performed spalling tests are shown in Fig.16.

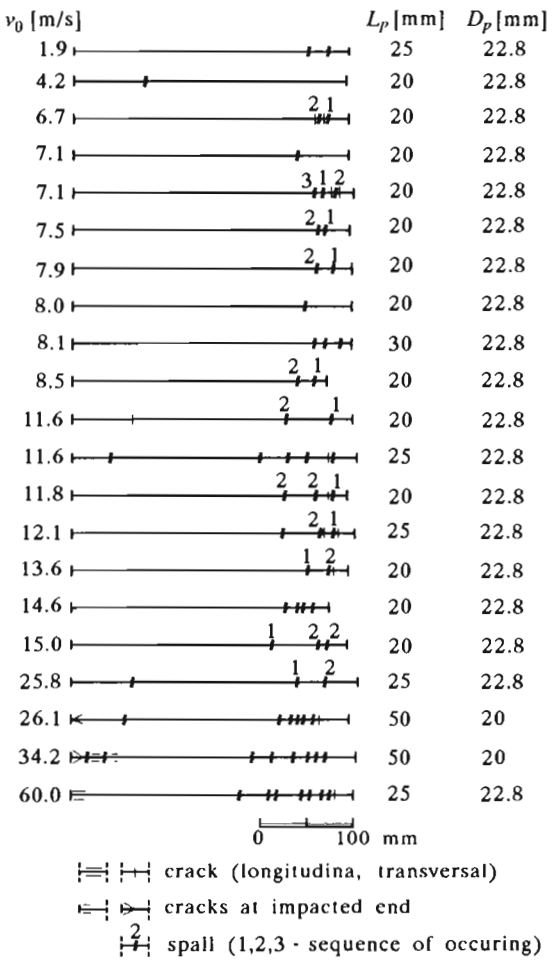

Fig. 16. Effect of impact velocity on multiple spalling in microconcrete bars

5. Dynamic shearing

The new experimental technique for shear testing at high strain rates is based on dynamic loading of a shear specimen which is places in a special shear device. The principle of arrangement of the simple shear device is presented in the Fig.17. It consists of two coaxial cylindrical parts. The external part is tubular with cylindrical inner section and hexagonal outer section. Its height is 45 mm and is reinforced to be able to fix the specimen firmls. The internal part is massive. It is 25.4 mm in diameter and its height is 45 mm. Both

are composed of two symmetrical parts, between which the sheet in testing is fixed using screws of high endurance. Two bands of the specimen between the internal and external parts of the device are in plane shear when these cylinders move axially one toward another. The width of these bands is 3 mm. Each band before test is rectangle and become very near to parallelogram having the length and the height constant. The specimens can have different thickness. There are two kinds of specimens: one is made of the steel XES (chemical composition: C-50, Ni-25, Cr-18, Mn-189, Cu-23, Al-57, Si-4, P-17 in 10^{-3} volume percent, thickness 0.74 mm) and the other is of steel 1H18N9T (chemical composition: C-10, Mn-200, Si-80, P-5, S-3 Cr-180, Ni-80, thickness 0.5 mm).

First, the system is tested under quasi-static loading for verifying the effectiveness (cf Gary and Nowacki (1994); Nowacki and Nguyen Huu Viem (1995)). The presence of free bounds of specimen results in the heterogeneity of stress field because the stress vector normal to the free surfaces must be zero, therefore we have assumed that the dimensions of the perturbed zone were small comparing to the dimensions of the specimen. This assumption is acceptable as shown by Gary and Nowacki (1994), where the mounting of the sheet is tested and the homogeneity of the deformation field is observed. In general, we must take the ratio a_0/l_0 sufficiently small. It is by Rauch and G'Sell (1989), Tourabi et al. (1993) that when the ratio $a_0/l_0 < 1/10$, the results of test were good for both static and dynamic cases. We take in our tests $a_0/l_0 = 1/10$.

The device with specimen (4) is placed between two bars of the standard SHPB – see Fig.1. Note that in this case the mechanical impedance of the shear device and the SHPB must be the same to avoid the interface parasite signal. The much more higher velocity of loading can be realised using only one bar of the SHPB. The impulse is created by the third projectile bar – the usual compression technique. We have to register the input, transmitted and reflected impulses: $\varepsilon_I, \varepsilon_T$ and ε_R. In the axis shown in Fig.17 the stress tensor has the following components: σ_{11}, σ_{22} and σ_{12}. The presence of σ_{11} and σ_{22} is due to the fact that $a = a_0 = \text{const}$. The strain tensor has only one non-zero component $\varepsilon_{12} = \gamma$. In this test, large deformations can be obtained, in contrast to the case of torsion of thin cylindrical specimens (cf Hartley et al. (1987)). The specimens deformed quasi-statically or dynamically to $70 \div 100\%$, observed under the optical microscope, have the similar structure. The traversal lines marked on the specimens before the test remain parallel after the test.

In the complete analysis, we must take into account that the loading of the specimen is not instantaneous. The loading compressing wave takes some

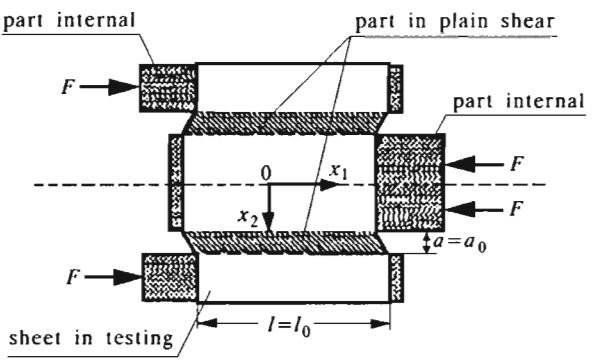

Fig. 17. Principle of the arrangement

time to transmit from one end to the other end of the device. However, we have reached in our tests very good equilibrium of forces on two sides of the shear device, see Gary and Nowacki (1994). We observe that the input force and the output were very similar in shape neglecting the small oscillations of the input force. So, in the simplified analysis we suppose that the loading is homogeneous and the quasi-static approach can be applied. Knowing the velocities on bounds of the system we can find the displacements. The force is taken to be equal to the mean value of input and output forces. The exceptional quality of the homogeneity of the residual strain field show that the simplified analysis can be used in the zone of plastic deformations.

The analogous boundary-value problem of the simple shear was formulated by Nowacki and Nguyen Huu Viem (1995). We consider the rate-independent constitutive relations for adiabatic process with combined isotropic-cinematic hardening at moderate pressures (cf Nguyen Huu Viem (1985)). The thermal expansion, the heat of elastic deformation and the heat of internal rearrangement are neglected. The program ABAQUS was used by Nowacki and Nguyen Huu Viem (1995) in the numerical simulation of the posed problem. We see for example the heterogeneity of the strain and stress fields at the free bounds of the specimen at the distance less than 5% of the total length when the strain is 70%, exactly as in the experiments. For example, for the steel 1H18N9T the zone of heterogeneity of the stress fields σ_{12} and σ_{11} and the mesh are shown in the Fig.18.

In conclusion an exceptional homogeneity of the permanent strain field at finite deformations over the total length of the specimens is observed in experiments and in results of simulation.

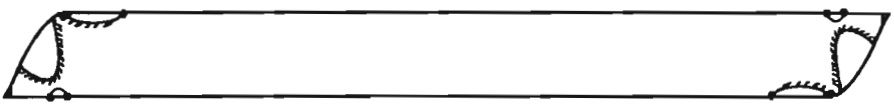

Fig. 18. Simple shear of 1H18N9T steel – zones of heterogenity

6. Conclusions

Four kinds of Hopkinson bar type impact tests were presented: compression, Taylor, spalling, and shear tests. Two types of tests, i.e., compression and spalling were used here for determination of the behaviour and the strength of brittle materials at high strain rates. Two remaining ones were used for determining dynamic properties of metals.

The experimental arrangements for the measurement of force, displacement and temperature data under loading at high strain rates, presented in this work, make possible to investigate various solids; like, concrete, rocks, ceramics, as well as, alloys or steels, in various modes, using only the standard SPHB and meeting the basic requirements of a simple specimen geometry and lack of on-specimen strain gauges. Low costs of the non-instrumented specimens allow large experimental series, resulting in proper distinction between the scatter of material characteristics and the errors of measurement and evaluation.

Acknowledgements

This paper was supported by the State Committee for Scientific Research (KBN), Project No. 7 T07A 026 08 on "Dynamic fracture of materials".

References

1. BAUER J., 1982, Considerations on the Design of a Stiff Testing Machine, *Studia Geotechnica et Mechanica*, **4**, 3-4, 3-14
2. BHARGAVA J., REHNSTROM A., 1977, Dynamic Strength of Polymer Modified and Fiber-Reinforced Concretes, *Cement and Concrete Research*, **7**, 198-208
3. BIERWIRTH S., NAJAR J., 1992, Experimental Apparatus for Measuring the Dynamic Tensile Strength of Elastic-Brittle Materials, XXIX Polish Conference of Solid Mechanics, Rytro
4. BUCHAR J., DUSEK F., 1975, The Influence of Loading Rate on Mechanical Properties of Rocks, *Arch. Górnictwa*, **20**, 2, 245-259

5. CAZENEUVE C., MAILE J.C., 1985, Etude du comportement da composites a fibres de carbonne sous differentes vitesses de deformation, *J. Physique*, **46**, 8, 551-556

6. CHOU S.C., ROBERTSON K.D., RAINEY J.H., 1973, The Effect of Strain Rate and Heat Developed During Deformation on the Stress-Strain Curve of Plastics, *Exp. Mech.*, **13**, 10, 422-432

7. CHRISTENSEN R.J., SWANSON S.R., BROWN W.S., 1972, Split Hopkinson Bar Tests on Rock under Confining Pressure, *Exp. Mech.*, **12**, 1, 500

8. GARY G., NOWACKI W.K., 1994, Essai de cisaillement plan applique a des totes minces, *J. de Physique IV*, Coll. C8, **4**, 65-70

9. HARTLEY K.A., DUFFY J., HAWLEY R.H., 1987, Measurement of the Temperature Profile during Shear Band Formation in Steels Deforming at High Strain Rates, *J. Mech. Phys. Solids*, **35**, 3

10. KLEPACZKO J., 1971, The Modified Hopkinson Bar, (in Polish), *Mech. Teoret. i Stos.*, **9**, 4, 479-497

11. KLEPACZKO J., 1983, On the Rate Sensitivity of Coal, *Rozpr. Inż.*, **31**, 3, 341-360

12. KLEPACZKO J.R., KRUSZKA L., 1994, Review of Experimental Techniques for Metals at High Strain Rates in Tension, Report No. 2/94/LPMM, Metz University

13. KRUSZKA L., NOWACKI W.K., 1995, Thermoplastic Analysis of Normal Impact of Long Cylindrical Specimen (Experiment and Comparsion with the Numerical Calculation), *J. of Thermal Stresses*, **18**, 313-334

14. KRUSZKA L., NOWACKI W.K., WOLNA M., 1988, Experimental Investigations of Fracture Mechanisms in Brittle Photoelastic Materials, *Proc. VII European Conference on Fracture*, Budapest, vol 2, 523-525

15. KRUSZKA L., NOWACKI W.K., WOLNA M., 1992a, Static and Dynamic Tests on Brittle Photoelastic Material, (in Polish), *IFTR Reports*, **3**

16. KRUSZKA L., NOWACKI W.K., WOLNA M., 1992b, Strength and Fracture Analysis of Brittle Photoelastic Material. Static and Dynamic Tests, *Eng. Trans.*, **40**, 3, 343 -362

17. KRZYSZTOŃ D., MIKOS T., STEWARSKI E., 1986, Investigation of Rock Sample Dynamic Properties on the Hopkinson Modified Bar Device, *Arch. Górnictwa*, **31**, 4, 661-688

18. LINDHOLM V.S., YEAHLEY L.H., NAGY A., 1974, The Dynamic Strength and Fracture Properties of Drosser Basalt, *Int. J. Rock Mech. Min. Sci.*, **11**, 181-191

19. LUNDBERG B., 1976, A Split Hopkinson Bar Study of Energy Absorption in Dynamic Rock Fragmentation, *Int. J. Rock Mech. Min. Sci.*, **13**, 187-197

20. MAIDEN C.J., GREEN S.J., 1966, Compressive Strain-Rate Tests on Six Selected Materials at Strain Rates from 10^{-3} to 10^{4} in/in/sec, *J. Appl. Mech.*, September, 496-504

21. MALVERN L.E., JENKINS D.A., TANG T., ROSS C.A., 1986, Compressive Split Hopkinson Bar Testing of Concrete, *Proc. the Int. Symp. on Intense Dynamic Loading and Its Effects*, Science Press, Beijing, China, 726-731

22. NAJAR J., 1994, Dynamic Tensile Fracture Phenomena at Wave Propagation in Ceramic Bars, *J. De Physique IV,* Coll. C8, **4**, 647-652

23. NGUYEN HUU VIEM, 1985, Qualitative Analysis of Propagation of Isothermal and Adiabatic Acceleration Waves in the Range of Finite Deformations, *Arch. of Mech.,* **37**, 439-447

24. NOWACKI W.K., NGUYEN HUU VIEM, 1995, Dynamic Simple Shear Test. Experiment and Numerical Investigation, Technical Report DYMAT-9-TC, Munich,

25. RAUCH E.F., G'SELL C., 1989, Flow Localisation Induced by a Change in Strain Path in Mild Steel, *Material Sic. and Eng.,* A111, 71

26. TOURABI A., WACK B., GUELIN P., FAVIER D., PEGON P., NOWACKI W.K., 1993, Remarks on an Experimental Plane Shear Test and on an Anisotropic Elastic-Plastic Theory, 12th International Conference SMIRT, Session L, Stuttgart

27. WOLNA M., KRUSZKA L., 1991, Brittle Photoelastic Materials in the Investigations of Stress and Strain States, (in Polish), *IFTR PAS Reports,* **22**

Nowe zastosowania pręta Hopkinsona (w konfiguracji na ściskanie) do określania dynamicznych własności materiałów

Streszczenie

W artykule przedstawiono eksperymentalne wyniki testów na jednoosiowe ściskanie, rozciąganie i ściskanie cial kruchych i metali w zakresie wysokich prędkości odkształceń. W badaniach dynamicznych stosowano standardowe urządzenie pomiarowe, pręt Hopkinsona, posiadające pneumatyczną wyrzutnię cylindrycznych pocisków obciążających. W tej pracy zostały pokazane różne konfiguracje prętów pomiarowych Hopkinsona wraz z dodatkowym wyposażeniem badawczym. Umożliwiło to określenie dynamicznego zachowania się materiałów w różnych układach testujących przy wykorzystaniu tylko tego jednego stanowiska badawczego.

Manuscript received November 15, 1995; accepted for print December 5, 1995